Available online at www.sciencedirect.com

ScienceDirect

Geochimica et Cosmochimica Acta 303 (2021) 205–222

Geochimica et Cosmochimica Acta

www.elsevier.com/locate/gca

Changing inputs of continental and submarine weathering sources of Sr to the oceans during OAE 2

Lucien Nana Yobo [a,*], Alan D. Brandon [a], Chris Holmden [b], Kimberly V. Lau [c], James Eldrett [d]

[a] *Department of Earth and Atmospheric Sciences, University of Houston, Houston, TX, United States*
[b] *Department of Earth Science, University of Saskatchewan, Saskatoon, Canada*
[c] *Department of Geosciences and Earth and Environmental Systems Institute, The Pennsylvania State University, University Park, PA, United States*
[d] *Shell International Exploration and Production, the Netherlands*

Received 22 September 2020; accepted in revised form 10 March 2021; Available online 23 March 2021

Abstract

Ocean anoxic events (OAE) are characterized by increased organic content of marine sediment on a global scale with accompanying positive excursions in sedimentary organic and inorganic $\delta^{13}C$ values. To sustain the increased C exports and burial required to explain the C isotope excursion, increased supplies of nutrients to the oceans are often invoked during ocean anoxic events. The potential source of nutrients in these events is investigated in this study for Oceanic Anoxic Event 2, which spans the Cenomanian-Turonian boundary. Massive eruptions of one or more Large Igneous Provinces (LIPs) are the proposed trigger for OAE 2. The global warming associated with volcanogenic loading of carbon dioxide to the atmosphere has been associated with increased continental weathering rates during OAE 2, and by extension, enhanced nutrient supplies to the oceans. Seawater interactions with hot basalts at LIP eruption sites can further deliver ferrous iron and other reduced metals to seawater that can stimulate increased productivity in surface waters and increased oxygen demand in deep waters. The relative importance of continental and submarine weathering drivers of expanding ocean anoxia during OAE 2 are difficult to disentangle. In this paper, a box model of the marine Sr cycle is used to constrain the timing and relative magnitudes of changes in the continental weathering and hydrothermal Sr fluxes to the oceans during OAE 2 using a new high-resolution record of seawater $^{87}Sr/^{86}Sr$ ratios preserved in a marl-limestone succession from the Iona-1 core collected from the Eagle Ford Formation in Texas. The results show that seawater $^{87}Sr/^{86}Sr$ ratios change synchronously with Os isotope evidence for the onset of massive LIP volcanism 60 kyr before the positive C isotope excursion that traditionally marks the onset of OAE 2. The higher temporal resolution of the seawater Sr isotope record presented in this study warrants a detailed quantitative analysis of the changes in continental weathering and hydrothermal Sr inputs to the oceans during OAE 2. Using an ocean Sr box model, it is found that increasing the continental weathering Sr flux by ~1.8-times captures the change in seawater $^{87}Sr/^{86}Sr$ recorded in the Iona-1 core. The increase in the continental weathering flux is smaller than the threefold increase estimated by studies of seawater Ca isotope changes during OAE 2, suggesting that hydrothermal forcing may have played a larger role in the development of ocean anoxic events than previously considered

Keywords: Strontium isotopes; OAE; Weathering; Cretaceous

* Corresponding author.
E-mail address: lnanayobo@uh.edu (L. Nana Yobo).

https://doi.org/10.1016/j.gca.2021.03.013
0016-7037/

1. INTRODUCTION

Ocean Anoxic Events (OAE) are identified in the rock record by elevated concentrations of organic matter in marine sediments and positive shifts in sedimentary $\delta^{13}C$ values, a signal major perturbation to the Earth's exogenic C cycle from increased organic carbon burial (Schlanger and Jenkyns 1976; Sageman et al., 2006). One of the most studied examples is Ocean Anoxic Event 2 (OAE 2) spanning the Cenomanian-Turonian boundary (CTB) in the Late Cretaceous. The duration of OAE 2 is 600,000–800,000 years based on rhythmically bedded strata in the Western Interior Seaway (WIS) of North America (Sageman et al., 2006; Eldrett et al., 2015a; Jones et al., 2020). Traditionally, the length of the event is represented by the stratigraphic thickness of the positive $\delta\ ^{13}C_{org}$ excursion (CIE) of 2–5‰ (Scholle and Arthur 1980; Jenkyns, 2010). Two factors contribute to increased organic carbon burial: (1) higher preservation at the sediment water interface, which is enhanced during periods of expanded bottom water anoxia in the oceans (e.g., Ostrander et al., 2017), and/or (2) increased exports of primary produced organic matter from the photic zone, which is improved during periods of increased nutrient availability in the oceans (Jenkyns, 2010 and references therein). The relative importance of these two processes for OAE 2 is a frequent subject of study and debate (Blättler et al., 2011; Pogge von Strandmann et al., 2013 Owens et al., 2018; Them et al., 2018). Climate and ocean circulation models generally invoke increased continental weathering during OAE 2 as a key global change variable (e.g., Topper et al., 2011; Monteiro et al., 2012; Baroni et al., 2014) and are parameterized with continental weathering proxy studies, notably Ca and Li isotopes, to set the magnitude of the continental weathering (Blättler et al., 2011; Pogge von Strandmann et al., 2013). However, the proposed threefold increase in continental weathering fluxes of Ca to the oceans during OAE 2 proposed by Blättler et al. (2011) was based on Ca isotope records that could not be reproduced in a follow-up study by Du Vivier et al. (2015). The source and relative weight of increased supplies of nutrients to the oceans during OAE 2 is the subject of this study.

Early studies of OAE 2 (Schlanger and Jenkyns 1976; Demaison and Moore, 1980; Pedersen and Calvert, 1990) focused on climate and ocean circulation changes to explain increased total organic carbon (TOC) concentrations in marine sediments, highlighting the role of warmer Late Cretaceous climates and sluggish circulation may have played in the preservation and burial of marine organic matter. Warmer temperatures cause increased soil mineral weathering, resulting in increased weathering supplies of nutrients to the oceans that could then fuel additional productivity, organic carbon export, increased oxygen utilization in deep waters, and expanded bottom water anoxia–thereby leading to organic carbon burial (Schlanger and Jenkyns 1976; Demaison and Moore, 1980; Pedersen and Calvert, 1990). These studies, however, could not adequately account for the timing of OAE 2 before the evidence began to grow for its volcanic origin.

Increased submarine volcanism during OAE 2 is supported by episodic increases in trace metal abundances of basaltic affinity in carbonate sediments from the proto-North Atlantic region (Orth et al., 1993). The metal source was initially attributed to increased hydrothermal venting at mid-ocean ridges (Orth et al., 1993), but was quickly amended to massive submarine eruptions of one or more Large Igneous Provinces (LIPs), particularly the Caribbean Large Igneous Province (CLIP) in the eastern Pacific, which erupted near the Central American Gateway to the proto-North Atlantic Ocean (Sinton and Duncan, 1997). A submarine volcanic trigger is further supported by a global decrease in global seawater $^{87}Sr/^{86}Sr$ during OAE 2, and similar patterns for the other Cretaceous OAEs (Ingram et al., 1994; Bralower et al., 1997; Jones and Jenkyns 2001; Ando et al., 2009). The perturbations in the ocean Sr cycle offered a means by which the magnitude of the eruptions and the volumes of seawater that interacted with hot basalt during LIP magmatic activity could be assessed (Ingram et al., 1994). However, the response of the ocean Sr cycle to the volcanic trigger was expected to be sluggish on account of the long modern oceanic Sr residence time (2.5 Ma; Hodell et al., 1990), adjusted to 1.35 Myr in this study using updated continental input Sr fluxes from Peucker-Ehrenbrink and Fiske (2019). The poorly resolved record of changing seawater $^{87}Sr/^{86}Sr$ in the Late Cenomanian and early Turonian challenged the ability to more definitively determine shifts to the Sr cycle. Moreover, there were competing effects to the ocean Sr mass balance needs to be considered—most notably the higher continental weathering fluxes of Sr to the oceans that would drive the $^{87}Sr/^{86}Sr$ ratio of seawater in the opposite direction to that produced by increased volcanism on the ocean floor.

In contrast to Sr, the marine Os cycle shifted very abruptly from a continental weathering-dominated signature to a mantle-dominated signature, consistent with a massive magmatic event near the onset of OAE 2 (Turgeon and Creaser, 2008; Du Vivier et al., 2014; Jones et al., 2020). With its much shorter ocean residence time (3–50 kyr; Oxburgh 2001) compared to Sr (~1.35 Myr) the eruptions could be shown to have started *ca.* 20–60 kyr before the positive CIE and the onset of OAE 2. However, the LIP-induced ocean Os cycle perturbation was so large that it completely overwhelmed any increase in continental weathering of Os to the oceans that may have also occurred in response to global warming driven by volcanogenic carbon dioxide emissions.

The relative importance of continental weathering and submarine volcanic delivery of nutrients to the oceans during OAE 2, and the time scales over which they played a role in its development, remain open questions, but can be partially constrained by strontium isotope records. This is because evolution of seawater $^{87}Sr/^{86}Sr$ reflects changes in two principle input Sr fluxes to the oceans: (1) venting of hydrothermal fluids from active submarine volcanism that deliver basaltic-derived micronutrients (Fe, Mn, Cu, Co, Zn) and Sr with a modern $^{87}Sr/^{86}Sr$ ratio of ~0.7031 (Snow et al., 2005), and (2) rivers and groundwater draining the continental crust that delivers the important macronu-

trient, phosphate, to the oceans and Sr with a modern $^{87}Sr/^{86}Sr$ that has been estimated at 0.7110 (Palmer and Edmond 1989; Richter et al., 1992). The latter has been recently adjusted to 0.71040 to reflect the most recent comprehensive study of continental sources of Sr to the oceans (Peucker-Ehrenbrink and Fiske, 2019) The higher $^{87}Sr/^{86}Sr$ of the continental weathering input reflects the higher $^{87}Rb/^{86}Sr$ ratio of the continental crust. It's older rock ages and higher Rb concentrations yield higher production rates of ^{87}Sr from radioactive decay of ^{87}Rb, compared to the mantle-source region (0.7025–0.7037) that melts to produce the oceanic crust (Wickman, 1948). Using simple mixing and the present-day seawater $^{87}Sr/^{86}Sr$ of 0.7092 (Elderfield, 1986), modern Sr input fluxes to the oceans from continental weathering and submarine weathering by hydrothermal fluids is estimated at 84% and 16%, respectively. The relative size of the inputs has changed over geological time. Periods of increased mountain building correlate with higher $^{87}Sr/^{86}Sr$ ratios of seawater while periods of rapid seafloor spreading and LIP eruptions correlate with lower ratios (Palmer and Edmond 1989; Richter et al., 1992). Carbonates of igneous and metamorphic origin in mountain uplift regions can also deliver large quantities of Sr to the oceans with high $^{87}Sr/^{86}Sr$ ratios (Derry and France-Lanord 1996; Jacobson et al., 2002).

Documented decreases in carbonate $^{87}Sr/^{86}Sr$ ratios during OAE 2 suggests that submarine hydrothermal inputs were a more dominant factor than increased continental weathering inputs (Ingram et al., 1994; Bralower et al., 1997; Jones and Jenkyns 2001; Snow et al., 2005). A seawater $^{87}Sr/^{86}Sr$ record for OAE 2 that is more precise and of higher temporal resolution than those currently available (Ando et al., 2009) could help to quantify the relative change in the Sr inputs. To address this issue, a new high-resolution record of seawater $^{87}Sr/^{86}Sr$ ratios for OAE 2 is presented in this paper from the Iona-1 core (Eldrett et al., 2014; Minisini et al., 2018), which samples a succession of pelagic marine carbonates from the Eagle Ford Formation in Texas. A forward box model of the ocean Sr cycle is implemented in combination with a conceptual model of how continental weathering and hydrothermal inputs of Sr likely would have responded to a massive episode of LIP volcanism. The result is an estimate for the continental weathering flux increase of Sr to the oceans during OAE 2 (and by inference Ca and nutrients) that is smaller than previous estimates (Blättler et al., 2011; Pogge von Strandmann et al., 2013).

2. GEOLOGIC SETTING

The Iona-1 core was drilled on a carbonate shelf at the southern gateway to the WIS in present-day southwest Texas (29°13.51′N, 100°44.49′W). The core recovered 180 m of Lower Cenomanian to Lower Coniacian marine sediment composed of marls and shales, with intermittent bentonite of the Boquillas Formation of the Eagle Ford Group (Eldrett et al., 2014). Sedimentation was slow and assumed to be relatively continuous during OAE 2 in the study setting (Eldrett et al., 2015a). An age model for the Iona-1 core was constructed from rhythmically deposited inter-bedded limestones and marlstones that were interpreted to reflect orbitally forced on sedimentation patterns and is supported by U-Pb zircon dating of bentonite beds (Eldrett et al. 2014, 2015a, 2015b; Minisini et al., 2018). The onset of the CIE in the Iona-1 core has recently been picked at 112.45 m based on the presumed first increase towards more positive $\delta\ ^{13}C_{org}$ values (i.e., Eldrett et al., 2015a; Eldrett et al., 2017; Minisini et al., 2018; Sullivan et al. 2020). However, there is some uncertainty in the exact placement of the start of OAE 2 CIE as the increase in $\delta\ ^{13}C_{org}$ is subtle over a few meters reflecting the continuous sedimentation over this interval compared to other sections (i.e., Pueblo, CO, USA). This uncertainty was highlighted by Eldrett et al. (2014; 2015b) with some authors placing the start of the CIE at 110.01 m (Jenkyns et al. 2017). This study follows the Jenkyns et al. (2017) placement of the onset of OAE 2 in the Iona-1 core. The interbedded marls are predominantly finely laminated and organic-rich in the lower Eagle Ford and become more bioturbated up core (Eldrett et al., 2014). Stratigraphic patterns in the traces of burrowing organisms and the diversity of benthic foraminifera documented periods of alternating oxic to dysoxic and aoxic bottom waters in the study area during OAE 2. Intervals of organic-rich laminated sediment and elevated trace metal nutrients are associated with bottom water anoxia (Eldrett et al., 2014, 2015a; Minisini et al., 2018), The depth of deposition is interpreted to be consistently below storm wave base in a restricted, sediment-starved setting (100–200 m depth; Eldrett et al, 2014). The decrease in initial $^{187}Os/^{188}Os$ begins ~60 kyr prior to the onset of the positive C isotope excursion that traditionally marks the base on OAE 2 and, consistent with recently published Os isotope evidence supporting the volcanic trigger hypothesis for OAE 2 (Du Vivier et al., 2014, Jones et al., 2020). The carbonate fraction of the sediment is mostly original low magnesium calcite mud derived from planktic foraminifera and calcispheres. Further details on the sedimentology, stratigraphy, and hydrographic conditions can be found in Eldrett et al., (2014, 2015a, 2017) and Minisini et al. (2018).

3. ANALYTICAL TECHNIQUES

3.1. Sample dissolution

Samples were collected approximately every 25 cm for Sr isotope analysis in the study interval of the core. The mixed limestone-marlstone-siliciclastic lithology of the Iona-1 core makes it important to use an acid that will dissolve carbonate minerals precipitated from seawater but will not appreciably attack and release Sr from non-carbonate minerals with higher or lower $^{87}Sr/^{86}Sr$ ratios. The dissolution procedure employed in this study has two sequential steps: (1) an ammonium acetate wash to remove Sr from exchange sites on clays and broken mineral surfaces from grinding, and (2) dissolution of the carbonate fraction of the sediment in buffered acetic acid (e.g. Bailey et al., 2000; Li et al., 2011).

In detail, 5 mL of 1 M ammonium acetate solution was added to 200 mg of rock powder for 12 hours after which

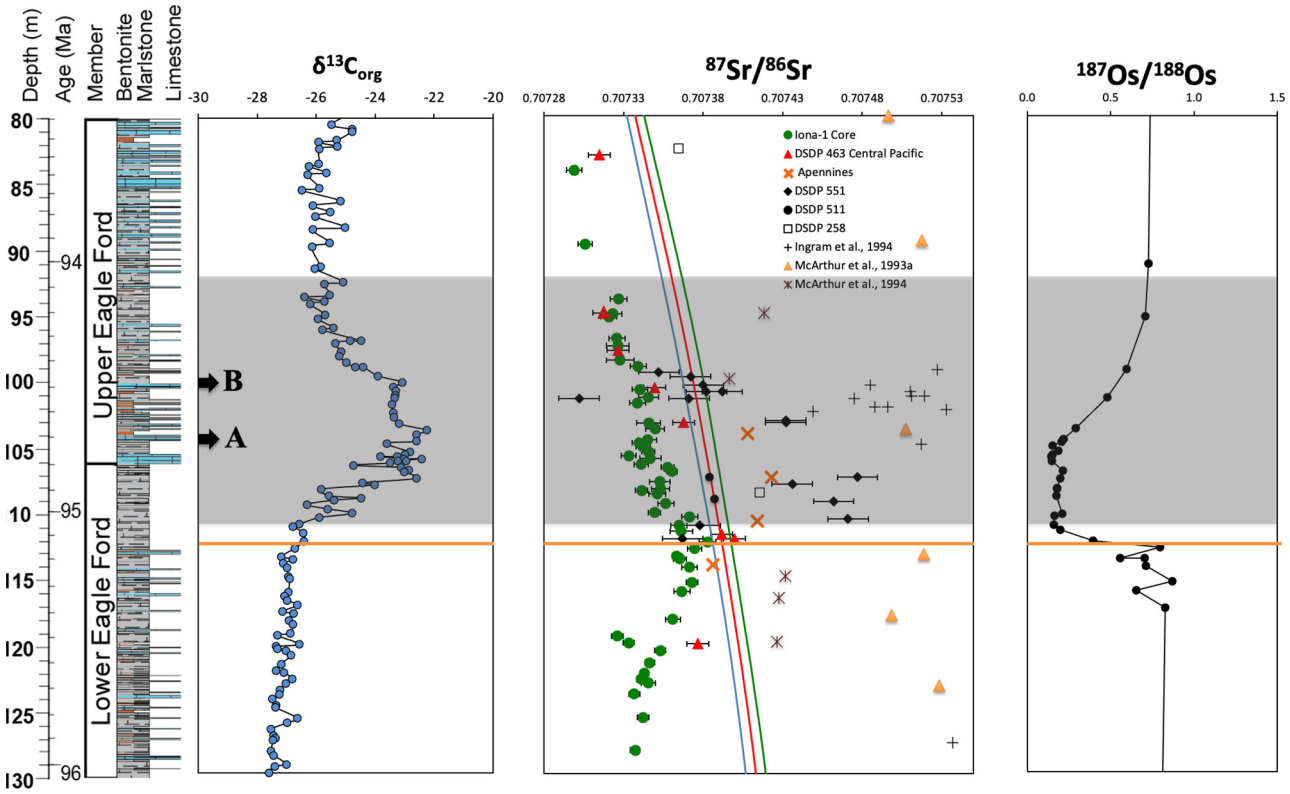

Fig. 1. $\delta^{13}C_{org}$ and $^{87}Sr/^{86}Sr$ ratios (see Table 1) for samples from the Iona-1 core. The OAE 2 interval is shaded in gray, based on the shift to more positive $\delta^{13}C_{org}$ relative to background values (modified from Eldrett et al., 2014). Os isotope data are from Sullivan et al. (2020). Published $^{87}Sr/^{86}Sr$ data from other locales (McArthur et al., 1993b; 1994; Ingram et al., 1994; Bralower et al., 1997; Frijia and Parente, 2008; Ando et al., 2009). The blue, red and green lines represent the seawater $^{87}Sr/^{86}Sr$ minimum, mean and maximum values, respectively, of the LOWESS curve (McArthur et al., 2012). Error bars represent ± 2SE uncertainty. The orange line indicates the onset of the shift to less unradiogenic $^{87}Sr/^{86}Sr$ ratios. "A" represents the first inflection point where the massive volcanism at the onset of OAE2 begins waning, as indicated by the rise in $^{187}Os/^{186}Os$ ratios. B is the second inflection point coincident with the decrease of organic carbon burial in ocean sediments, signally a start of the return to pre-excursion $\delta^{13}C_{org}$. (For interpretation of the references to colour in this figure legend, the reader is referred to the web version of this article.)

sample was centrifuged, the supernatant decanted, and the sample rinsed three times with ultrapure water. The samples were then immersed in 5 mL of 1 M buffered Optima glacial grade acetic acid for 1–2 hours at room temperature to dissolve carbonate minerals. The leachate was separated from the residue by centrifugation. The solution was then dried down and the acetate removed by redissolving the sample in a few mL of 6 N nitric acid (HNO_3) and dried down again. This step was repeated three times to ensure that acetate was decomposed. The residues were then dissolved in 0.45 N HNO_3 and transferred to pre-weighed acid-cleaned 50 mL centrifuge tubes. An aliquot of the stock solution was used for the analysis of elemental concentrations by inductively coupled plasma mass spectrometry (ICPMS) and inductively-coupled optical emission mass spectrometry (ICP-OES). Another aliquot was passed through a column containing Eichrom Sr Spec resin to purify Sr from Ca and other matrix elements prior to mass spectrometric analysis using thermal ionization mass spectrometry (TIMS).

3.2. Analytical techniques

Major and trace element concentrations were determined by ICP-OES and ICP-MS, respectively, at the University of Houston. Analytical uncertainty is generally better than ±5% 1σ, monitored by repeated analysis of an internal standard. The $^{87}Sr/^{86}Sr$ ratios were measured using a on a Thermo Scientific Triton Plus TIMS at the University of Houston using a multi-static measurement technique adapted from a method for obtaining high precision Nd isotopic ratios (Bennett et al., 2007). The measurement procedure begins with a slow increase of the filament temperature during which time the Sr ion beams are located, tuned, and peak-centered multiple times until a stable ^{88}Sr ion beam intensity of 6 V is reached. Three sets of Sr isotopic ratios were collected in each cycle (3 scans), with 10 cycles per block and 14 blocks per run, for a total of 420 measurements of $^{88}Sr/^{86}Sr$, $^{87}Sr/^{86}Sr$ and $^{84}Sr/^{86}Sr$. Mass 85 was monitored to correct $^{87}Sr/^{86}Sr$ for ^{87}Rb interference, but Rb beams were too small to warrant any significant

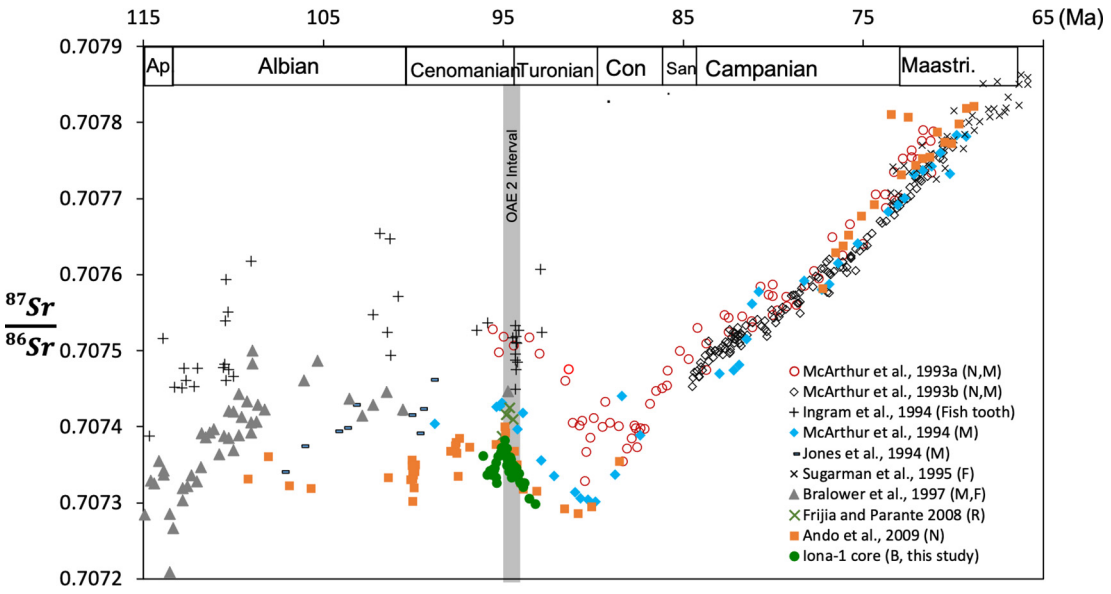

Fig. 2. Compilation of Late Cretaceous $^{87}Sr/^{86}Sr$ data against time (GTS 2020) showing the landscape of changing $^{87}Sr/^{86}Sr$ over time (modified from Ando et al., 2009). All $^{87}Sr/^{86}Sr$ data have been recalibrated to SRM 987 0.710251 (this study). Data from other sources are fitted to the new timescale by simply updating the originally proposed numerical ages for the stage boundaries reported in age model of the paper. F = foraminifera; M = macrofossil; N = nannofossil chalk; R = rudists, B = bulk carbonate.

corrections. The $^{87}Sr/^{86}Sr$ ratios were corrected for instrumental mass fractionation using a $^{86}Sr/^{88}Sr$ ratio of 0.1194.

The external precision for $^{87}Sr/^{86}Sr$ is ±5 ppm (2σ) base on repeated measurements of the SRM 987 standard yielding 0.710251 ± 2.951E−06 (n = 20) over the course of this work.

4. RESULTS

4.1. Elemental concentrations

Trace element concentrations were used to screen the leachates for non-carbonate sources of Sr by monitoring co-release of Al and Rb that are high in detrital clay minerals but low in marine carbonates (Tribovillard et al., 2006). The low Al concentrations (average ~200 ppm) in the leachates indicate that the ammonium acetate rinse of the sample powders and the weak acetic acid used to dissolve carbonate minerals resulted in a very minor release of Al from the samples (see supplements Table S1). The Al concentrations in the leachates are consistent with those of modern pure carbonate sediments where the main source of Al is from seawater itself (Veizer, 1983). As a point of comparison, Veizer (1983) reports 4600 ppm Al in pure marine carbonates, which is higher than concentrations measured in this study, and much lower than concentrations of ~80,000 ppm in shales. The low Al concentrations in the sample leachates is strong evidence for negligible release of Sr from non-carbonate minerals.

Manganese can also reside in metalliferous coatings on sediment grains. Although the concentration of Sr is insignificant in these coatings (Veizer, 1983), sample leachates with elevated Mn concentrations may still record seawater $^{87}Sr/^{86}Sr$ ratios. Higher Mn concentrations in carbonates deposited in the proto-North Atlantic region during OAE 2 (Pratt et al., 1991) reflect higher oceanic inventories of Mn, due to the reduction in the size of the oxic marine sink where Mn-oxides would have normally accumulated, and increased Mn fluxes from hydrothermal weathering of the LIP basalts (Orth et al., 1993; Sinton and Duncan, 1997; Snow et al., 2005). However, the Mn concentrations recorded in the carbonate fractions of the Iona-1 core are relatively low.

4.2. Sr isotopes

The carbonate $^{87}Sr/^{86}Sr$ profile in the Iona-1 core (Fig. 1 and listed in Table 1) is a smoothly varying function of stratigraphic depth. This meets the expectation for a sedimentary succession with no major depositional hiatuses, for an element like Sr with a long oceanic residence time. The overall trend is one of increasing $^{87}Sr/^{86}Sr$ before OAE 2 followed by a decreasing trend in the early part of OAE 2, a period of no change in $^{87}Sr/^{86}Sr$ in the middle part of OAE 2, and a resumption of the declining trend in $^{87}Sr/^{86}Sr$ for the remainder of OAE 2. In detail, the shift from increasing to decreasing $^{87}Sr/^{86}Sr$ ratios near the onset of OAE 2 occurs at the same stratigraphic level as the decrease in $^{187}Os/^{188}Os$ ratios signaling the massive increase in LIP volcanism. The ~150 kyr of no change in $^{87}Sr/^{86}Sr$ occurs in a stratigraphic interval marked by the beginning of the post-volcanic rise in oceanic $^{187}Os/^{188}Os$ ratios, and the end of the peak positive shift in sedimentary $\delta^{13}C$ values (Fig. 1). Carbonate $^{87}Sr/^{86}Sr$ ratios continue to decline for ~2.5 Myr after OAE 2, until about the end of the Turonian, at which point they being to increase again.

Table 1
Measured $^{87}Sr/^{86}Sr$ isotope ratios of the Iona-1 core.

Stratigraphic height (m)	Age	87Sr/86Sr	2 s.e.
80.25	93.25	0.707299	4.90E−06
85.31	93.59	0.707306	4.46E−06
89.32	93.84	0.707327	5.11E−06
90.57	93.90	0.707323	5.59E−06
90.83	93.92	0.707321	5.07E−06
92.73	94.02	0.707326	5.07E−06
93.44	94.05	0.707326	6.90E−06
94.73	94.12	0.707328	8.80E−06
95.32	94.14	0.707339	5.02E−06
97.41	94.25	0.70734	4.95E−06
98.08	94.28	0.707346	6.28E−06
98.56	94.31	0.707339	5.19E−06
100.30	94.40	0.707346	7.43E−06
100.90	94.43	0.70735	5.94E−06
101.83	94.48	0.707345	5.80E−06
102.21	94.49	0.70734	4.50E−06
102.63	94.51	0.707342	4.44E−06
102.95	94.53	0.707345	4.08E−06
103.33	94.55	0.707333	4.76E−06
103.54	94.56	0.707347	6.85E−06
104.18	94.59	0.707341	4.56E−06
104.44	94.60	0.707357	4.04E−06
104.83	94.62	0.707361	3.18E−06
105.68	94.67	0.707353	6.46E−06
106.45	94.70	0.707353	5.69E−06
106.50	94.71	0.707341	3.88E−06
106.94	94.73	0.707351	5.28E−06
107.82	94.77	0.707356	5.09E−06
108.77	94.81	0.707349	3.85E−06
109.22	94.83	0.707371	4.97E−06
110.01	94.87	0.707365	5.14E−06
110.49	94.90	0.707366	7.09E−06
111.36	94.94	0.707383	5.11E−06
111.88	94.97	0.707375	4.47E−06
112.45	95.01	0.707363	3.03E−06
112.77	95.02	0.707365	3.96E−06
113.42	95.06	0.707372	4.90E−06
114.50	95.13	0.707373	3.75E−06
115.45	95.17	0.707367	5.09E−06
118.16	95.30	0.707361	4.57E−06
119.77	95.37	0.707326	3.66E−06
120.40	95.41	0.707333	3.45E−06
121.09	95.44	0.707353	3.51E−06
122.18	95.50	0.707346	3.01E−06
123.14	95.54	0.707343	2.91E−06
123.68	95.57	0.707341	2.89E−06
124.03	95.59	0.707345	4.45E−06
125.13	95.64	0.707337	3.42E−06
127.31	95.75	0.707342	3.65E−06
130.17	95.90	0.707337	3.14E−06
135.25	96.15	0.707362	6.09E−06

5. DISCUSSION

Before interpreting the $^{87}Sr/^{86}Sr$ trend in the Iona core, it is important to consider the likelihood that it genuinely reflects secular change in seawater $^{87}Sr/^{86}Sr$ during OAE 2, rather than stratigraphic changes in diagenetic or local Sr cycling effects.

5.1. Diagenetic effects

Seawater derived Sr can be difficult to extract from mixed carbonate/siliciclastic lithologies without also releasing Sr from the detrital silicates. The ion exchange wash and weak acetic acid dissolution used in this study appears to have successfully targeted the release of Sr from carbonate minerals, based on the low Al concentrations in the acid leachates. A more difficult problem is the diagenetic transfer of silicate derived Sr into new carbonate mineral growth. However, there are a number of factors to consider that make recrystallization of the carbonates in the Iona core potentially less of a problem than in carbonate sediments from other settings. Firstly, the source of the carbonate mud is pelagic calcifiers (i.e. foraminifera and coccolithophores) that produce low magnesium calcite (LMC), which is the most diagenetically stable calcium carbonate polymorph. Secondly, the sediments have low permeability, and the observed carbonate cements have been interpreted to have precipitated in close diagenetic system (Eldrett et al., 2015b, Minisini et al., 2018). Accordingly, any cements that formed would likely re- incorporate seawater-derived Sr released to the pore fluids. Oxygen isotopes in the Iona-1 core show no obvious evidence for recrystallization of carbonates, such as low $\delta^{18}O$ values indicative of higher temperatures encountered during deep burial, or meteoric waters (Eldrett et al., 2015b). The bulk carbonate $\delta^{13}C$ and $\delta^{18}O$ values in the Iona-1 core are similar to well preserved calcite tests of calcite foraminifera reported in other locations of the WIS (Eldrett et al., 2015b and references therein). Hence, the $^{87}Sr/^{86}Sr$ ratios in the carbonate fractions were likely not altered by diagenetic processes. Hence it is concluded that the $^{87}Sr/^{86}Sr$ in the carbonate fractions measured here were unlikely to be reset by post-depositional diagenetic processes.

5.2. Local Sr cycling effects

Even in cases where diagenetic effects are negligible and the sample dissolution procedure only releases seawater-derived Sr from the samples, marine carbonates deposited in epeiric seas may record $^{87}Sr/^{86}Sr$ ratios that are different from the global ocean due to circulation restrictions and local Sr cycling. The study setting is located at the southern gateway to the WIS—an epeiric seaway that did not support a typical mid-Cretaceous marine fauna (McArthur et al., 1994, Eldrett et al., 2017, Minisini et al., 2018). Moreover, the WIS experienced climate oscillations that affected precipitation and freshwater inputs from rivers. These changes, in turn, affected salinity patterns, water column stratification and mixing in the Seaway, while longer term changes in sea level could eased or restrict the flow of water over the sill at the southern and northern gateways (Holmden et al., 1997a, 1997b; Cochran et al., 2003). The long length of the Seaway, equivalent to the distance between the present-day Arctic and Gulf of Mexico, increases the likelihood that local Sr cycling effects could be important in different parts of the Seaway at different times. The Late Cenomanian eustatic sea-level rise, and the location of the study setting near the southern gateway

to the WIS lend support to improved circulation in the southern part of the Seaway during OAE 2. As an additional consideration, the large difference in the Sr concentration between seawater and river waters dictates that the salinity must typically decrease to below ~15‰ before the local $^{87}Sr/^{86}Sr$ of brackish seawater can begin to deviate significantly from the global ocean $^{87}Sr/^{86}Sr$ ratio (Andersson et al., 1992; Holmden et al., 1997a, 1997b; Holmden and Hudson, 2003). However, some forms of submarine groundwater discharge (SGD) have the potential to change seawater $^{87}Sr/^{86}Sr$ ratios without any appreciable adjustments of salinity (Beck et al., 2013). A large Sr flux from SGD was likely important in the Late Cretaceous WIS in South Dakota (Cochran et al., 2003).

The role of local Sr cycling effects in the Seaway setting of the Iona-1 core is best evaluated with records from nearby locales in the WIS where circulation restriction is more likely—but these records do not exist. With spatially distributed records, a gradient in seawater $^{87}Sr/^{86}Sr$ ratios, if present, could be used to reveal locations affected by local Sr cycling and the direction of change in local seawater $^{87}Sr/^{86}Sr$ ratios compared the open ocean ratio. Until more local/regional records are available, the only remaining option is to compare the Iona-1 record to other published records regardless of their location. To do so, the records presented here were re-normalized to the SRM 987 ratio of 0.710251 obtained in this study (Figs. 1 and 2).

All but one of the published $^{87}Sr/^{86}Sr$ records are inconsistent with the record of the Iona-1 core presented in this study. They are also inconsistent with each other (Fig. 1). Most of the published records depict higher inferred seawater $^{87}Sr/^{86}Sr$ ratio during OAE 2. The Iona-1 core record gives lower $^{87}Sr/^{86}Sr$ ratios than the LOWESS curve of seawater $^{87}Sr/^{86}Sr$ (McArthur et al., 2012). Well-preserved rudists collected from near shore deposits representing shallow water settings in the Southern Apennines during OAE 2 (Frijia and Parente, 2008) gave even higher $^{87}Sr/^{86}Sr$ ratios than the LOWESS curve. These results were interpreted to reflect Sr inputs from local rivers, implying brackish waters and salinity stratification in this setting (Frijia and Parente, 2008). The $^{87}Sr/^{86}Sr$ ratios spanning OAE 2 are also high in several Deep Sea Drilling Project Sites (DSDP) Site 511 (Falkland Plateau South Atlantic; Bralower et al., 1997), DSDP Site 258 (Naturaliste Plateau, Indian Ocean; Bralower et al., 1997), DSDP Site 551 (Goban Spur, North Atlantic; Bralower et al., 1997), and the ODP Site 763B (Exmouth Plateau, Indian Ocean; Bralower et al., 1997). The carbonates in these deposits are primarily planktonic foraminifera that appear to have been altered (cf. Bralower et al., 1997). Although the data are sparse, the $^{87}Sr/^{86}Sr$ ratios from Site 511 overlap those from the Iona-1 core immediately before OAE 2, but then shift to relatively high $^{87}Sr/^{86}Sr$ ratios in the early stages of OAE 2 before decreasing again in the latter stages. The English Chalk (McArthur et al., 1993a) has the highest $^{87}Sr/^{86}Sr$ ratios before OAE 2 of any of the published records and a decrease in $^{87}Sr/^{86}Sr$ during OAE 2 that is broadly consistent with the Iona-1 core record offset to higher ratios.

The $^{87}Sr/^{86}Sr$ record of OAE 2 that best matches the Iona-1 core is from DSDP Site 463, a carbonate succession draping the margin of a mid-Pacific atoll (Ando et al. 2009). Although the DSDP Site 463 data are sparse in the OAE 2 interval, $^{87}Sr/^{86}Sr$ ratios are consistently lower than the other published records. Like the Iona-1 core and English Chalk, carbonate $^{87}Sr/^{86}Sr$ ratios increase before OAE 2 and decrease after the onset of OAE 2. However, the low sampling resolution of the DSDP Site 463 record does not permit a confirmation of the 150 kyr interval of no change in seawater $^{87}Sr/^{86}Sr$ in the middle of OAE 2 that is present in the Iona-1 core record. To reconcile Site 463 with other published records, Ando et al. (2009) conceded that sections of the record could be shifted to lower $^{87}Sr/^{86}Sr$ ratios due to carbonate recrystallization in the presence of altered pore waters generated by water-rock interactions with basaltic volcanic rocks located at the base of the carbonate succession. The implications being that Sr bearing fluids may have migrated upwards through the sediment as a result of compaction and/or heating from below (Richter and Liang, 1993). However, the similarly low $^{87}Sr/^{86}Sr$ ratios found in the Iona-1 core in the WIS, which is not underlain by basaltic volcanic rocks, indicate that these interactions were either inconsequential or did not happen at Site 463. Neither does it seem likely that Sr released into pore fluids from altered volcanic ash beds is responsible for lowering the carbonate $^{87}Sr/^{86}Sr$ ratios in the Iona-1 core, as it would have to then be concluded that the similarities between the two records are a coincidence.

In summary, local Sr cycling effects could be responsible for the poor reproducibility observed in some shallow water carbonate records of changing $^{87}Sr/^{86}Sr$ ratios during OAE 2 (cf. Frijia and Parente, 2008). Other $^{87}Sr/^{86}Sr$ records may have been altered during diagenesis (McArthur et al., 1993a; Bralower et al., 1997). Contamination of seawater derived Sr from lithogenic Sr released from detrital silicates has been recognized as problem hampering accurate reconstructions of seawater $^{87}Sr/^{86}Sr$ ratios using bulk carbonate sediments for a long time, which is why carbonate fossils have been used instead (e.g., Veizer, 1983; Montanez et al., 1996; Young et al., 2009; Edwards et al., 2015; El Meknassi et al., 2018). If investigated in a systematic way in future studies, local Sr cycling effects can provide important information on circulation patterns and the general hydrography of epeiric seas like the WIS during OAE 2. At present, the reliability of the promising similarities between the $^{87}Sr/^{86}Sr$ records of the Iona-1 core and DSDP Site 463 core to gauge the likelihood that the more detailed record of the Iona-1 core accurately records changes in the $^{87}Sr/^{86}Sr$ ratio of the oceans during OAE 2.

5.3. Key patterns of change in seawater $^{87}Sr/^{86}Sr$ during OAE 2

LIP eruptions have been implicated to cause decreases to lower seawater $^{87}Sr/^{86}Sr$ ratios in the Cretaceous, including OAE 2 (Ingram et al., 1994; Jones and Jenkyns, 2001), but this is the first time that a decrease in carbonate $^{87}Sr/^{86}Sr$ ratios has been shown to occur synchronously with the decrease in seawater initial $^{187}Os/^{188}Os$ ratios. This suggests a casual effect where the hydrothermal weathering of the LIP basalts delivered large quantities of Sr to the

oceans, beginning *ca.* 60 kyr before the onset of OAE 2 (Fig. 1). Continental weathering is assumed to have also increased the flux of Sr to the oceans during OAE 2, but its effect on the seawater $^{87}Sr/^{86}Sr$ ratio is likely to be masked by the stronger change in Sr inputs from submarine volcanism. However, when the Os isotopes begin to shift back to baseline, indicating waning of submarine volcanism, the continental weathering flux of Sr may become visible again in the seawater $^{87}Sr/^{86}Sr$ record. The stratigraphic interval of arrested change in the carbonate $^{87}Sr/^{86}Sr$ record may signal the timing of this effect. These nuances in the seawater $^{87}Sr/^{86}Sr$ record are used to estimate the sizes of the continental and hydrothermal input Sr-flux changes to the oceans during OAE 2 using an ocean Sr box model.

A unique solution for any change in seawater $^{87}Sr/^{86}Sr$ is difficult to determine. For example, an increase in seawater $^{87}Sr/^{86}Sr$ can be produced by: (1) increasing the continental weathering Sr flux, (2) decreasing the hydrothermal Sr flux, or (3) increasing the $^{87}Sr/^{86}Sr$ ratio of the continental weathering flux. Accordingly, there are multiple ways to produce every change in seawater $^{87}Sr/^{86}Sr$ and they are not mutually exclusive. Accordingly, a conceptual model with additional geological constraints is needed to implement the box model. For example, an invariant hydrothermal flux during OAE 2 is not in accordance with the evidence for submarine volcanism during the event and can therefore be ruled out (Turgeon and Creaser 2008; Jenkyns, 2010; Du Vivier et al., 2014; Sullivan et al., 2020). Reducing the continental weathering flux of Sr can generate the declining trend in seawater $^{87}Sr/^{86}Sr$ ratio during OAE 2, but this is inconsistent with global warming predicted from volcanic outgassing of carbon dioxide, which should have accelerated continental weathering (Snow et al., 2005; Jenkyns, 2010). The Sr flux input from hydrothermal and continental weathering likely both increased in the early stages of OAE 2, as discussed above, but the hydrothermal inputs must have increased more to produce the early declining trend in seawater $^{87}Sr/^{86}Sr$. It is reasoned that any further changes in the apportioning of the Sr flux inputs in the midst of OAE 2 should also lead to changes in the slope of the $^{87}Sr/^{86}Sr$ trend with time, if the relative flux change in one input is not overwhelmed by the relative flux change in the other.

As indicated above, there are two subtle changes of slope in the seawater $^{87}Sr/^{86}Sr$ trend with time that occur in the middle of OAE 2 signaling the first time since the beginning of the eruptions, that the continental weathering Sr flux is no longer completely dominated by the hydrothermal Sr flux. The first inflection point occurs at the 105 m depth (labeled A in Fig. 1) where massive volcanism ends or dramatically declines, as indicated by the rise in $^{187}Os/^{186}Os$ ratios (Fig. 1). Above this level the $^{187}Os/^{188}Os$ ratio of seawater steadily increases, favoring a shift to greater relative inputs of Os from continental weathering. The second, stratigraphically higher inflection point occurs at 100 m depth (labeled B in Fig. 1), coincident with the termination or dramatic decrease of organic carbon burial in ocean sediments, as signaled by the start of the return to pre-excursion $\delta\ ^{13}C_{org}$ As increased organic carbon burial in the oceans during OAE 2 is at least partly tied to increased continental weathering inputs of nutrients needed to fuel additional productivity, the decline in $\delta\ ^{13}C_{org}$ values at the end of OAE 2 is a logical place to expect continental flux perturbation.

Two additional constraints underpin the modeling. Firstly, after terminating the continental weathering Sr flux perturbation terminates at 105 m (label A Fig. 1), the $^{87}Sr/^{86}Sr$ ratio of seawater must continue to steadily decline for another 1 million year (Fig. 1) after OAE 2. The second constraint relates to the rising trend in seawater $^{87}Sr/^{86}Sr$ before OAE 2, (124–114 m), representing ~500 kyr of time before the eruption of the LIP that drove seawater $^{87}Sr/^{86}Sr$ in the opposite direction. Whether the rising trend before the LIP eruptions was due to increased continental weathering inputs, decreased hydrothermal inputs, or some combination of the two cannot be uniquely determined. And yet the choice made here could affects the outcome of the forward modeling, specifically the relative magnitudes of the modeled Sr flux increases from continental weathering and hydrothermal venting during OAE 2. As it is not known which scenario is correct, two forward models of seawater $^{87}Sr/^{86}Sr$ changes during OAE 2 are produced, resulting in two estimates of the change in the continental weathering input of Sr to the oceans during OAE 2 (Fig. 3A, B).

5.4. Estimating Sr flux perturbations to the oceans during OAE 2

A box model is used to quantify the perturbations of the ocean Sr cycle that can account for the observed changes in seawater $^{87}Sr/^{86}Sr$ ratio during OAE 2. A coupled Sr mass and Sr-isotope mass balance approach is used here. Parameters are based on modern values, adjusted for the Cretaceous based on available constraints that are described in detail below.

The time dependent change in the inventory of Sr in the oceans is represented by Eq. (1),

$$\frac{dN_{Sr}}{dt} = J_{riv} + J_H + + J_{dia} - J_{ppt} \tag{1}$$

where N_{Sr} represents moles of Sr in the oceans and J_{riv}, J_H, J_{dia} and J_{ppt} are the riverine (i.e. continental weathering), hydrothermal, diagenetic and carbonate precipitation fluxes, respectively. The corresponding $^{87}Sr/^{86}Sr$ ratio of the seawater is given by Eq. (2),

$$\frac{dR^{Sr}_{SW}}{dt} = \frac{J^{Sr}_{riv}\left(R^{Sr}_{riv} - R^{Sr}_{SW}\right) + J^{Sr}_{H}\left(R^{Sr}_{H} - R^{Sr}_{SW}\right) + J^{Sr}_{Dia}\left(R^{Sr}_{Dia} - R^{Sr}_{SW}\right)}{N_{Sr}} \tag{2}$$

where R^{Sr}_{SW} represents the $^{87}Sr/^{86}Sr$ ratio of the ocean Sr reservoir and R^{Sr}_{riv}, R^{Sr}_{H}, and R^{Sr}_{Dia} are the $^{87}Sr/^{86}Sr$ ratios of the riverine, hydrothermal, and diagenetic Sr inputs, respectively.

Initial $^{87}Sr/^{86}Sr$ ratios and Sr input fluxes were obtained from present-day estimates (Table 2) with several adjustments that are explained below. The output flux of Sr depends on the N_{Sr} and is parameterized using a first-order rate constant calculated from the initial conditions.

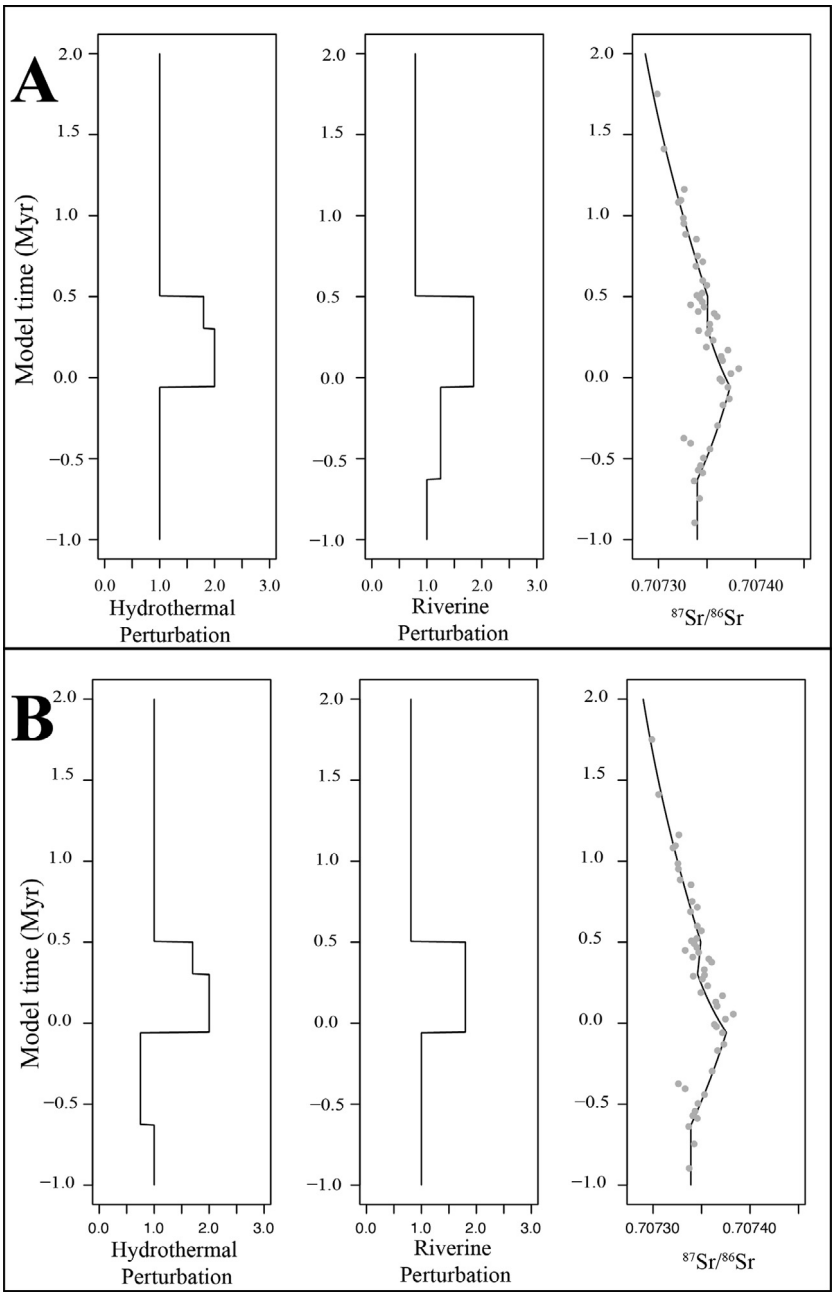

Fig. 3. Box model results of the perturbations in hydrothermal and riverine Sr fluxes needed to simulate the change in seawater $^{87}Sr/^{86}Sr$ ratios during OAE 2 reconstructed using the Iona-1 core. The flux perturbations are normalized to the Sr fluxes that define the pre-OAE 2 steady-state ocean Sr cycle indicted between −1 and −0.65 Myr model-time (Table 2). The LIP eruptions begin at time zero in model-time. The onset of the C-isotope excursion begins 60 kyr later. (A) The increasing trend in seawater $^{87}Sr/^{86}Sr$ before OAE 2 is modeled by increasing the continental weathering input Sr flux by 1.25-times. At 0.0 Myr, a 2-times increase in the hydrothermal inputs Sr flux and a 1.85-times increase in the continental input Sr flux yields the observed decreasing trend in $^{87}Sr/^{86}Sr$ that begins with the onset of the LIP eruptions. Subsequently, the decreasing trend is arrested for a period of 150 kyr beginning at 0.350 Myr model-time in the record, which is coincident with the evidence for waning volcanism in the seawater Os isotope record. To create the observed change in the slope for this 150 kyr period, the perturbation in the hydrothermal Sr input flux is decreased to 1.8-times and the continental weathering flux Sr input is decreased to 0.79 times. This combination of flux changes keeps then seawater $^{87}Sr/^{86}Sr$ decreasing at the end of OAE 2, when the hydrothermal Sr input flux is returned to the pre-OAE 2 values at the end of the peak interval of elevated $\delta^{13}C$ values at 0.5 Myr. (B) The increasing trend in seawater $^{87}Sr/^{86}Sr$ before OAE 2 is modeled by decreasing the hydrothermal Sr input flux by 0.75-times. The hydrothermal Sr input flux is increased 2-times, and the continental Sr input flux is increased 1.8-times at the beginning of the LIP eruptions. The 150 kyr interval of no change in seawater $^{87}Sr/^{86}Sr$ is created by decreasing the hydrothermal Sr input flux perturbation to 1.8-times and the continental weathering Sr-flux perturbation to 0.81-times. The hydrothermal Sr input flux is returned to the pre-OAE 2 baseline value at the end of the peak interval of elevated $\delta^{13}C$ values.

Table 2
Comparison of modern ocean Sr budgets with inferred boundary conditions for the OAE 2 models.

	Modern							Late Cretaceous[8]			
	ocean Sr budget							Ocean Sr budget			
	min	Sr	max	min	87Sr/86Sr	max	ref.	change[7]	Sr	87Sr/86Sr	ref.
Reservoir		moles							moles		
Seawater Sr		1.25E+17			0.70918		2		**1.25E+17**	**0.70733**	1
Sr residence time (My)		1.48							1.35		
Sr Fluxes		10^9 mol/y			value or weighted avg.				10^9 mol/y		
global rivers		47.6			0.71107		3				
SGD	7	17.5	28		0.7089		3				
global rivers + SGD	54.6	65.1	75.6		0.71049						
riverine volcanic ash dissolution		1			0.705		3				
eolian volcanic ash dissolution	0.0114	0.017	0.0228		0.705		3				
all continental sources	55.6	66.1	76.6		0.71040				**66.1**	**0.70791**	
diagenetic		5.5			0.70849		3		**5.5**	**0.70733**	
all non hydrothermal Sr inputs	61.1	71.6	82.1		0.71026		3		71.6	0.70786	1
hydrothermal Sr inputs[1]		12.7		0.7025	0.7031	0.7037	3	1.65	**20.9**	**0.7055**	4,5
carbonate precipitation output		84.3					1		**92.5**		1

1. This study; measured or calculated from mass balance.
2. Richter et al. (1992).
3. Peucker-Ehrenbrink and Fiske (2019).
4. Bickle and Teagle (1992), Kawahata et al. (2001).
5. Antonelli et al. (2017).
6. Coogan and Dosso (2012).
7. 1.65 times increased sea floor spreading rate; Berner, 1994; 3.8 times increased Sr concentration in the middle Cretaceous oceans (cf. Antonelli et al., 2017).
8. Bolded values are used in the model simulations of this paper.

As with many box models, steady state is assumed prior to running the model.

Two revisions were made to the modern ocean Sr budget to account for differences in the Late Cretaceous Sr cycle. First, the $^{87}Sr/^{86}Sr$ ratio of all continental sources of Sr (the riverine flux, submarine groundwater discharge, and terrestrial volcanic sources are combined into the J_{riv}) was adjusted from the present-day ratio of 0.71040 down to 0.70791 in order to achieve a steady-state $^{87}Sr/^{86}Sr$ ratio for Late Cretaceous seawater representing a period of unchanging $^{87}Sr/^{86}Sr$ ratios at the base of the study core (Fig. 1). This is not meant to imply that the ocean Sr cycle was truly in steady state at this time, but rather, to give a set of initial conditions against which changes in ocean Sr cycling that occur above this level in the core can be compared to. Second, the background hydrothermal flux was increased by 65% in accordance with reconstructions of higher Cretaceous seafloor spreading rates compared to the modern (Berner 1994). It is assumed that Late Cretaceous N_{Sr} was comparable to the modern reservoir of size of 1.25×10^{17} moles of Sr, which gives a residence time of 1.35 Myr (Table 2). Multiple limes of evidence suggest that the Sr concentration of seawater was higher in the Late Cretaceous than today (Steuber and Veizer, 2002; Coogan 2009; Antonelli et al., 2017; Akhtar et al., 2020; Zhang and DePaolo, 2020) and consequently, the oceanic Sr residence time was longer than today. To investigate the sensitivity of the model results to higher seawater Sr concentration, the model is run for various Sr reservoir size up to 5-times larger than modern, which corresponds to a residence time >5 Myr.

The ocean Sr cycle is forced by changing one or both of the two largest input Sr fluxes to the oceans, J_{riv} and J_H. A step-change in either flux causes an initially relatively quick change in the $^{87}Sr/^{86}Sr$ ratio of seawater that slows exponentially with time as it approaches the steady state $^{87}Sr/^{86}Sr$ ratio within five residence times (~7 Myr). Because OAE 2 lasts for maximum of ~800 kyr, none of the flux perturbations employed to simulate the trend in seawater $^{87}Sr/^{86}Sr$ ratio during OAE 2 occurs long enough for the ocean Sr cycle to reach steady state.

The simulations show that the continental weathering flux of Sr to the oceans increased by 1.8-times the value of the modern Sr flux of 66.1 x 10^9 moles/y (Table 2). depending on how the rising trend in seawater $^{87}Sr/^{86}Sr$ is treated before OAE 2 is treated as discussed in Section 6.3 (Fig. 3). The slightly lower estimate is the result of treating the increasing trend in seawater $^{87}Sr/^{86}Sr$ before OAE 2 as the effect of increasing continental weathering inputs of Sr to the oceans and constant hydrothermal inputs. The slightly higher estimate treats the increasing trend in seawater $^{87}Sr/^{86}Sr$ before OAE 2 as the effect of decreasing hydrothermal fluxes of Sr to the oceans and constant continental weathering inputs. These results are effectively the same and show that how the increase in $^{87}Sr/^{86}Sr$ before OAE 2 is treated does not significantly affect the result. On the other hand, it is important to bear in mind that the model results only consider changes in the input fluxes of Sr to the oceans and make the assumption that the $^{87}Sr/^{86}Sr$ ratio of the continental weathering flux was constant. Considering that OAE 2 occurred near the peak of the Late Cenomanian transgression, if the flux-weighted average $^{87}Sr/^{86}Sr$ ratio of the continental weathering flux changed during OAE 2, it would have likely increased due to the drowning of carbonate platforms with low $^{87}Sr/^{86}S$ ratios. If this is correct, then the increase in the continental weathering flux of Sr to the oceans would have been lower than the results shown in Fig. 3.

By considering the sensitivity of the model results to differences in initial conditions, it is unlikely that the continental weathering flux of Sr to the oceans during OAE 2 is underestimated. Moreover, assuming that the increase in continental Sr flux scales proportionately to the continental Ca, Li and nutrient fluxes, the smaller continental weathering response to the LIP eruption suggested here—compared to previous estimates of a threefold increase (Blättler et al., 2011; Pogge von Strandmann et al., 2013)— has important implications for the ocean eutrophication model of OAE 2, where the expansion of ocean anoxia and increased burial of organic carbon is largely driven by increased productivity that is stimulated by increased continental weathering supplies of nutrient phosphate to the oceans (see below). The lower continental weathering response elevates the importance of other contributing factors to anoxia, such as the role played by reduced metals and gases to the oceans from the LIP eruptions (Sinton and Duncan, 1997), the paleogeography and circulation of the proto-North Atlantic nutrient trap and its surrounding epeiric seas (Trabucho-Alexandre et al., 2010), positive feedbacks related to P-recycling efficiency (Ingall and Jahnke, 1994), and more organic carbon burial due less efficient remineralization in anoxic bottom waters (increased preservation).

The Iona-1 record shows decreasing seawater $^{87}Sr/^{86}Sr$ ratios continuing after the cessation of OAE 2. Because the forcing from excess Sr input from LIP volcanism and the continental weathering flux perturbation was removed near the end of OAE 2, the expectation is that seawater $^{87}Sr/^{86}Sr$ ratio of seawater should eventually reverse and reach to a new higher steady-state $^{87}Sr/^{86}Sr$ ratio after about five residence time. Instead, it continues falling with no evidence of change at the end of OAE 2. This pattern can be modeled to produce a new steady state by decreasing the hydrothermal input Sr flux to the oceans at the end of the peak interval of the CIE or by decreasing the continental weathering Sr flux. The latter is favored here, because excess hydrothermal inputs of Sr to the oceans is expected to end in concert with the relaxation of initial $^{187}Os/^{186}Os$. One other possibility is that the $^{87}Sr/^{86}Sr$ ratio of continental weathering decreased around this time. This would require large changes in the types of continental rocks exposed to weathering, which is unlikely on short time scales. It is even less likely that the hydrothermal Sr flux would change without first signaling a change in seawater initial $^{187}Os/^{186}Os$, so a reduction in the continental weathering input is the favored explanation.

Published records show that the declining trend in seawater $^{87}Sr/^{86}Sr$ continued for 2.5 Myr until about the end of the Turonian (Fig. 2). Thereafter, $^{87}Sr/^{86}Sr$ ratios rise steeply for the next ~25 Myr, consistent with a first order decrease in ridge-crest hydrothermal activity in the oceans

(Berner, 1994). The increasing trend in seawater $^{87}Sr/^{86}Sr$ is the dominant trend over the Late Cretaceous period, which continues into the Cenozoic (Vérard et al., 2015). It is therefore the intervals of decreasing seawater $^{87}Sr/^{86}Sr$ that are anomalous when considering the broader time frame (Jones and Jenkyns, 2001). This is evidence that continental weathering Sr flux inputs were either much smaller in the Late Cretaceous than they are today, or that hydrothermal Sr flux inputs were much larger (Ingram et al., 1994). These broader findings are mirrored in this more detailed study of ocean Sr cycle changes during OAE 2.

5.5. Additional considerations regarding ocean eutrophication and residence time

The ocean eutrophication model (Schlanger and Jenkyns 1976; Demaison and Moore, 1980; Pedersen and Calvert, 1990) predates the broader understanding of OAE 2 that has emerged in recent years. Most notably, it has been established that eruptions of one or more LIPs triggered the event (Turgeon and Creaser, 2008; Du Vivier et al., 2014; Sullivan et al., 2020), that the small and relatively secluded proto-North Atlantic Ocean functioned as nutrient trap (Trabucho-Alexandre et al., 2010), that records of environmental changes during OAE 2 from the proto-North Atlantic ocean and surrounding seas may give a distorted picture of the global change impacts, and that the Caribbean LIP erupted near the main oceanic gateway to the proto-North Atlantic in Central Americas (Fig. 1). The latter could expedite the delivery of: (1) trace metal nutrients to the proto-North Atlantic, most notably iron, which limits primary productivity even in nutrient replete regions of the modern oceans (Leckie et al., 2002; Monteiro et al., 2012), and (2) anoxic, intermediate depth waters to the proto-North Atlantic that could increase the preservation of exported organic matter from the photic zone and its burial in the proto-North Atlantic region, while over time increasing productivity and anoxia through the positive feedback involving sedimentary phosphorous recycling (Ingall et al., 1993). In other words, the eruption of Caribbean LIP would have increased organic carbon burial in the proto-North Atlantic basin without any increase in continental weathering rates during OAE 2. Additional considerations are needed to explain the geographic variability and magnitude of the OAE 2 C isotope excursion, which cannot simply be attributed organic carbon burial (Owens et al., 2018).

The modeled excess of hydrothermally sourced Sr to the oceans can be converted to implied volumes of new oceanic crust produced by the LIP eruption(s) that triggered OAE 2. For this, the modern estimated ridge-crest hydrothermal Sr exchange flux of 6×10^8 mol of strontium per cubic km of new crust is used (Ingram et al., 1994) is assumed to be broadly applicable to hydrothermal Sr exchange between seawater and LIPs (Table 3). A doubling of the hydrothermal Sr flux at the onset of OAE 2 (the forcing that is needed to match the $^{87}Sr/^{86}Sr$ data in Fig. 3A) would add 39.9 km^3 of additional new crust production per year on a global scale. Considering the duration of the model perturbation in the hydrothermal Sr flux of 450 kyr, this equates to 15.7 million km^3 of extra basalt production over the duration of OAE 2. The volume of basalts erupted by the Caribbean LIP was estimated by Larson (1991) to be 20.41 million cubic kilometers, indicating that there is enough basalt in the Caribbean LIP to account for the increase in hydrothermal Sr inputs. It seems unlikely that most of the Caribbean LIP (nearly 80%) would have erupted in this relatively short time frame. Larson (1991) documented other LIPs with similar eruption ages that could have also contributed hydrothermal Sr to the oceans, thus increasing the total volume of plateau basalt volcanism to 58.2 million cubic kilometers. Only 27% of this larger volume of LIP basalt would need to erupt in the estimated time frame of 450 kyr.

This calculation can provide insight into the likely residence time of Sr in the oceans during the Late Cretaceous and by extension, the Sr concentration of seawater. At higher residence times, a larger perturbation of the hydrothermal Sr flux, and therefore an unreasonably large volume of basalt, would be needed to effect significant changes in seawater $^{87}Sr/^{86}Sr$. This is illustrated by a sensitivity test of varying Sr reservoir sizes (Fig. 4) with the Late Cretaceous boundary conditions described in Table 2. For simplicity, the model is forced by an increase in continental weathering of Sr leading up to and during OAE 2, combined with the emplacement of 100% of the estimated volume of the Caribbean LIP erupted over the duration of OAE 2 (Table 3). As shown in Fig. 4, as the ocean Sr reservoir size progressively increases, the modeled changes in seawater $^{87}Sr/^{86}Sr$ become smaller, and it becomes increasingly difficult to match the magnitude of the observed decrease in $^{87}Sr/^{86}Sr$ during OAE 2 in the Iona-1 core. Accordingly, at the higher residence times considered in Fig. 4, a larger hydrothermal forcing—and by extension, a volume of basalt greater than the Caribbean LIP—would be required, representing an untenable scenario. In sum, this back-of-the envelope calculation indicates that despite estimates for higher Sr concentrations of Late Cretaceous oceans relative to the modern, which in some calculations are significantly larger by a factor of four to five (e.g., Renard, 1986; Wallmann, 2001; Steuber and Veizer, 2002; Holmden and Hudson, 2003; Coggon et al., 2010; Antonelli et al., 2017), the maximum reasonable Sr residence time is likely to not have been dramatically different.

The only way to maintain a high Sr concentration in seawater, and a reasonable oceanic residence time is to increase the throughput of Sr, in the oceans i.e., inputs and outputs of Sr would both have to increase relative to the modern. This could include higher Sr flux inputs from carbonate sources of Sr, including weathering of exposed carbonate platforms in epicontinental marine settings, diagenetic fluxes of Sr from carbonate dissolution, and submarine groundwater discharge in carbonate platform settings (Chaudhuri and Clauer 1986; Huang et al., 2011; Beck et al., 2013; Peucker-Ehrenbrink and Fiske, 2019; Danish et al., 2020), analogous to a process suggested to influence the Ca isotope composition of seawater (Holmden et al., 2012). The main benefit of higher carbonate dissolution fluxes is that there is little effect on the $^{87}Sr/^{86}Sr$ ratio of seawater if the weathered carbonates are, geologically, recently

Table 3
Calculated volume of oceanic plateau basalt equivalent from the **hydrothermal flux during OAE 2.**

				Doubling the hydrothermal flux			**100% eruption of Carrebean LIP**		
	Modern Sr 10^9 mol/y	ref.	change[3]	Sr Fluxes	10^9 mol/y	$^{87}Sr/^{86}Sr$	Sr Fluxes	10^9 mol/y	$^{87}Sr/^{86}Sr$
Continental	66.01	1		Continental	66.01	0.7079	Continental	66.01	0.7079
Hydrothermal	12.70	1	1.65	Hydrothermal	20.96	0.7055	Hydrothermal	20.96	0.7055
				Fraction of total input			Fraction of total input		
Ocean crust production rate (mol/Km^3)				Continental	0.76		Continental	0.76	
	6.00E+08	2		Hydrothermal	0.24		Hydrothermal	0.24	
Estimated Volume of	Km^3			Onset of OAE2[4]	mol/y		Onset of OAE2[4]	mol/y	
Carrebean LIP	2.04E+07	5		Hydrothermal	4.19E+10		Hydrothermal	4.82E+10	
				Crust Production	Km^3		Crust Production	Km^3	
				Background	34.93		Background	34.93	
				Background + LIP	69.85		Background + LIP	80.28	
				LIP	34.93		LIP	45.36	
				Production over OAE2	1.57E+07		Production over OAE2	2.04E+07	
				Fraction of CLIP	0.77		Fraction of CLIP	1.00	

1. Peucker-Ehrenbrink and Fiske (2019).
2. Ingram et al. (1994).
3. 1.65 times increased sea floor spreading rate; Berner (1994).
4. Values used in the model simulations of this paper.
5. Larson (1991).

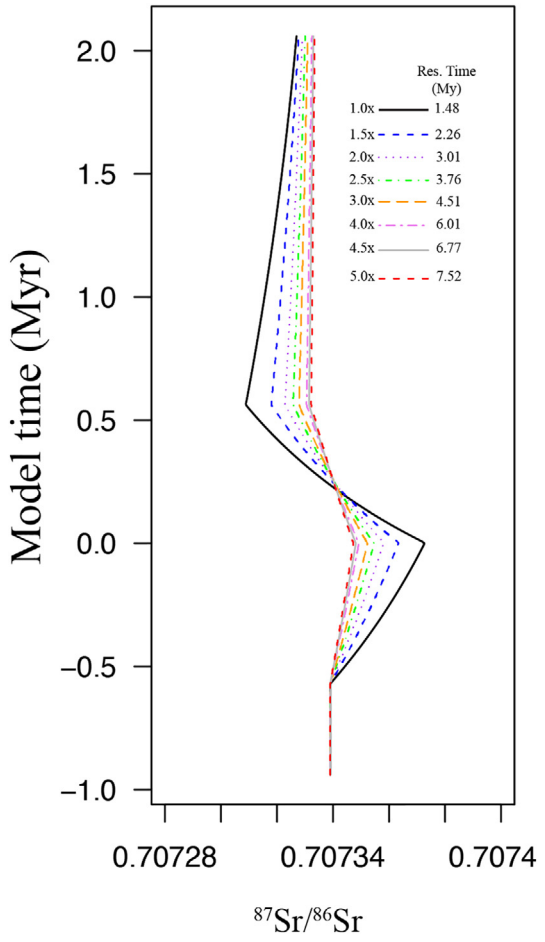

Fig. 4. Sensitivity of the box model to the marine residence time of Sr. The residence times reflect increasing the Sr reservoir size relative to the Late Cretaceous boundary conditions (Table 2) up to a residence time of about 7.52 Myr, five times longer than the baseline. The model is forced by increasing continental fluxes (Table 3) and an increase in hydrothermal flux during OAE 2 that is equivalent to the entirety of the Caribbean LIP being emplaced over OAE 2. As the residence time increases, the difference in modeled $^{87}Sr/^{86}Sr$ over OAE 2 becomes progressively smaller. At high residence times, it is impossible to match the decrease in $^{87}Sr/^{86}Sr$ without invoking unreasonable basalt eruption or considering other aspects of the Sr cycle. Onset of OAE 2 is at model time 0.

deposited. A second benefit of carbonate weathering is that it introduces the alkalinity that is needed to increase the removal of Sr from the oceans through increased carbonate precipitation rate. Another source of Sr to the oceans that was likely more important in the Cretaceous than it is today, is the submarine weathering of exposed basalt along the flanks of the mid-ocean ridges (cf. Cogné and Humler 2006). As the temperature of ocean bottom waters were much warmer in the Cretaceous (14 °C; Huber et al., 2002) than in present oceans (4 °C), the submarine weathering flux of Sr to the oceans could have been, at its maximum, twice as high as the modern flux (Beck et al., 2013; Peucker-Ehrenbrink and Fiske, 2019). In contrast to the carbonate dissolution/weathering fluxes, which affect the Sr concentration of seawater more than its $^{87}Sr/^{86}Sr$ ratio, low-temperature submarine weathering of basalt by warm ocean bottom waters would drive seawater to higher Sr concentrations (Coogan, 2009; Antonelli et al., 2017) and lower $^{87}Sr/^{86}Sr$ ratios (Ingram et al.,1994; Jones and Jenkyns, 2001; Ando et al., 2009).

The submarine weathering flux of Sr to the oceans prompts the consideration of additional, but related, assumptions that affects the impact of the validity of the calculations. The first one is that the box model, that is configured for this study, does not allow for any gain or loss of Sr during hydrothermal interactions between seawater and basalt. All Sr from seawater that enters the oceanic crust is exchanged, mole for mole, with basaltic Sr, which is then returned to seawater through venting. This is a common assumption that is made in most ocean Sr box models (Kristall et al., 2017). Recently, Antonelli et al. (2017) demonstrated that secular changes in the Mg and Ca concentrations of seawater affects the Sr exchange capacity of the oceanic crust. For example, the low concentrations of Mg in Cretaceous seawater results in lower fluxes of basaltic derived Sr to the oceans by about 20%, which results in higher predicted $^{87}Sr/^{86}Sr$ ratios for the hydrothermal flux. To account for this effect, a higher $^{87}Sr/^{86}Sr$ ratio of 0.7055 was used in this paper, for the hydrothermal flux of Sr to oceans during OAE 2 (Bickle and Teagle, 1992; Kawahata et al., 2001) rather than the more conventional $^{87}Sr/^{86}Sr$ ratio of 0.7025–0.7037. The latter range of ratios reflect the modern hydrothermal Sr flux, where all seawater Sr that circulated through the oceanic crust was exchanged for basaltic derived Sr due to the high present day Mg concentration of seawater.

While the data in this study support increased continental weathering inputs of Sr, Ca and nutrients to the oceans during OAE 2, the ~1.8-times increase suggested by Sr isotopes is lower than the threefold increase suggested by Ca isotopes (Blättler et al., 2011). The record and interpretation in that study have since been revised by Du Vivier et al. (2015). Another study using and $\delta^{7}Li$ as a continental weathering proxy is seemingly in agreement with the original Ca isotope study (Pogge von Strandmann et al., 2013). However, the origin of the negative Li isotope excursion upon which this estimate is based could have multiple interpretations. In fact, the decrease from 20 to 25‰ before OAE 2, to between 7 and 10‰ during OAE 2, overlaps $\delta^{7}Li$ values measured in high temperature hydrothermal fluids of 8‰ and in basalt from 5 to 7‰ (Sun et al., 2018). The authors, however, preferred a continental weathering source interpretation that related the change in Li isotopes in marine carbonates to the fractionation of Li isotopes during continental weathering in a period of enhanced (wet) hydrological cycle. In any case, the Li isotope effect is not a small one, and deserves to be followed up with additional study. In the meantime, climate and ocean circulation model studies are needed to examine the effects of the relatively smaller continental weathering flux increase of ~1.8-times found in this study.

6. CONCLUSIONS

A high-resolution record of change in the $^{87}Sr/^{86}Sr$ ratio of seawater during OAE 2 was reconstructed from the carbonate fraction of the Iona-1 core in the southern WIS. These new $^{87}Sr/^{86}Sr$ data fill in missing details for the $^{87}Sr/^{86}Sr$ seawater curve over this time interval, resolving questions about the timing and magnitude of change in hydrothermal and continental weathering fluxes of Sr to the oceans during OAE 2. Although submarine eruptions of LIPs have been implicated in the decrease in seawater $^{87}Sr/^{86}Sr$ during OAE 2, and other Cretaceous OAEs, for some time, this is the first time that the decrease $^{87}Sr/^{86}Sr$ is shown to have been synchronous with the decrease in the $^{187}Os/^{188}Os$ ratio of seawater, which is the benchmark proxy for tracing massive volcanism during OAE 2. The declining trend in seawater $^{87}Sr/^{86}Sr$ pauses in the middle of OAE 2 for about 150 kyr, which is interpreted to reflect the waning of submarine volcanism at this time, which allows effects of increased continental weathering fluxes of Sr to the oceans to become visible in the record of changing seawater $^{87}Sr/^{86}Sr$ for the first time since onset of OAE 2. An ocean Sr box model was employed simulate the change in seawater $^{87}Sr/^{86}Sr$ through OAE 2, and to quantify hydrothermal and continental weathering flux changes. The 1.8-times increase in the continental weathering flux during OEA 2 estimated using Sr isotopes in this study is smaller than threefold increase using Ca and Li isotopes as continental weathering proxies. This lower continental weathering rate has important ramifications for how OAE 2 and OAEs in general originate and evolve, and what controls nutrient delivery to the oceans during these events.

The modeling and overall conclusions, of this study also hinge on the assumption that the record of changing carbonate $^{87}Sr/^{86}Sr$ ratios in the Iona-1 core accurately records changes in seawater $^{87}Sr/^{86}Sr$ during OAE 2 and immediately before and after OAE 2 as well. The only way to test this assumption is to further examine the Sr record in other marine carbonate OAE 2 successions around the world at the same level of resolution. Finally, a forward model, such as the one employed in this study, helped to explore these relative changes but an inverse model could be used in future work to improve on the estimates presented here.

Declaration of Competing Interest

The authors declare that they have no known competing financial interests or personal relationships that could have appeared to influence the work reported in this paper.

ACKNOWLEDGEMENTS

We thank Shell International Exploration and Production Inc. for making samples available. LNY thanks Olivia Wren and Alex Heri for assistance in the laboratory. The manuscript was improved by suggestions of B. Peucker-Ehrenbrink and 2 anonymous reviewers. We also appreciate editorial handling by A. Jacobson. Funding for this project was made possible by National Science Foundation award EAR 1933302 to ADB and 1933298 to KVL as well as AAPG Student Grant-In-Aid (Kenneth H. Crandall Memorial Grant and Gustavus E. Archie Memorial Grant) and National GEM Consortium fellowship to LNY.

APPENDIX A. SUPPLEMENTARY MATERIAL

Supplementary data to this article can be found online at https://doi.org/10.1016/j.gca.2021.03.013.

REFERENCES

Akhtar A. A., Santi L. M., Griffiths M. L., Becker M., Eagle R. A., Kim S., Kocsis L., Rosenthal Y. and Higgins J. A. (2020) A record of the $\delta^{44/40}Ca$ and [Sr] of seawater Over the last 100 million years from fossil elasmobranch tooth enamel. *Earth Planet. Sci. Lett.* **543**.

Andersson P. S., Wasserburg G. J. and Ingri J. (1992) The sources and transport of Sr and Nd isotopes in the Baltic sea. *Earth Planet. Sci. Lett.* **113**, 459–472.

Ando A., Nakano T., Kaiho K., Kobayashi T., Kokado E. and Khim B.-K. (2009) Onset of seawater $^{87}Sr/^{86}Sr$ excursion prior to Cenomanian-Turonian oceanic anoxic event 2? New late Cretaceous strontium isotope curve from the central Pacific Ocean. *J. Foram. Res.* **39**, 322–334.

Antonelli M. A., Pester N. J., Brown S. T. and DePaolo D. J. (2017) Effect of paleoseawater composition on hydrothermal exchange in midocean ridges. *Proc. Natl. Acad. Sci.* **114**, 12413–12418.

Bailey T. R., McArthur J. M., Prince H. and Thirlwall M. F. (2000) Dissolution methods for strontium isotope stratigraphy: whole rock analysis. *Chem. Geol.* **167**, 313–319.

Baroni I. R., Topper R. P. M., van Helmond N. A. G. M., Brinkhuis H. and Slomp C. P. (2014) Biogeochemistry of the North Atlantic during ocean anoxic event 2: role of changes in ocean circulation and phosphorus input. *Biogeosciences* **11**, 977–993.

Bennett V. C., Brandon A. D. and Nutman A. P. (2007) Coupled ^{142}Nd-^{143}Nd isotopic evidence for Hadean mantle dynamics. *Science* **318**, 1907–1910.

Berner R. (1994) GEOCARB II: a revised model of atmospheric CO2 levels over Phanerozoic time. *Science* **249**, 1382–1386.

Beck A. J., Charette M. A., Cochran J. K., Gonneea M. E. and Peucker-Ehrenbrink B. (2013) Dissolved strontium in the subterranean estuary – Implications for the marine strontium isotope budget. *Geochim. Cosmochim. Acta.* **117**, 33–52.

Bickle M. R. and Teagle D. A. H. (1992) Strontium alteration in the Troodos ophiolite: implications for fluid fluxes and geochemical transport in mid-ocean ridge hydrothermal systems. *Earth Planet. Sci. Lett.* **113**, 219–237.

Blättler C. L., Jenkyns H. C., Reynard L. M. and Henderson G. M. (2011) Significant increases in global weathering during Oceanic Anoxic Events 1a and 2 indicated by calcium isotopes. *Earth Planet. Sci. Lett.* **309**, 77–88.

Bralower T. J., Fullagar P. D., Paull C. K., Dwyer G. S. and Leckie R. M. (1997) Mid-Cretaceous strontium-isotope stratigraphy of deep-sea sections. *GSA Bull.* **109**, 1421–1442.

Chaudhuri S. and Clauer N. (1986) Fluctuations of isotopic composition of strontium in seawater during the Phanerozoic eon. *Chem. Geol.* **59**, 293–303.

Cochran J. K., Landman N. H., Turekian K. K., Michard A. and Schrag D. P. (2003) Paleoceanography of the late Cretaceous (Maastrichtian) Western Interior seaway of North America: evidence from Sr and O isotopes. *Palaeogeogr. Palaeoclimatol. Palaeoecol.* **191**, 45–64.

Coggon R. M., Teagle D. A. H., Smith-Duque C. E., Alt J. C. and Cooper M. J. (2010) Reconstructing Past Seawater Mg/Ca and Sr/Ca from Mid-Ocean Ridge Flank Calcium Carbonate Veins. *Science* **327**, 1114–1117.

Cogné J.-P. and Humler E. (2006) Trends and rhythms in global seafloor generation rate. *Geochem. Geophys. Geosyst.* **7**.

Coogan L. A. (2009) Altered oceanic crust as an inorganic record of paleoseawatter Sr concentration. *Geochem., Geophys., Geosys.* **10**, Q04001.

Coogan L. A. and Dosso S. E. (2012) An internally consistent, probabilistic, determination of ridge-axis hydrothermal fluxes from basalt-hosted systems. *Earth Planet. Sci. Lett.* **323–324**, 92–101.

Danish M., Tripathy G. R. and Rahaman W. (2020) Submarine groundwater discharge to a tropical coastal lagoon (Chilika lagoon, India): An estimation using Sr isotopes. *Marine Chem.* **224** 103816.

Demaison G. J. and Moore G. T. (1980) Anoxic environments and oil source bed genesis. *AAPG Bull.* **64**, 1179–1209.

Derry L. A. and France-Lanord C. (1996) Neogene Himalayan weathering history and river 87Sr/86Sr impact on the marine Sr record. *Earth Planet. Sci. Lett.* **142**, 59–74.

Du Vivier A. D., Selby D., Sageman B., Jarvia I., Grocke D. and Voigt S. (2014) Marine $^{187}Os/^{188}Os$ isotope stratigraphy reveals the interaction of volcanism and ocean circulation during Oceanic Anoxic Event 2. *Earth Planet. Sci. Lett.* **389**, 23–33.

Du Vivier A., Jacobson A. D., Lehn G. O., Selby D., Hurtgen M. T. and Sageman B. B. (2015) Ca isotope stratigraphy across the Cenomanian-Turonian OAE 2: Links between volcanism, seawater geochemistry, and the carbonate fractionation factor. *Earth Planet. Sci. Lett.* **416**, 121–131.

El Meknassi S., Dera G., Cardone T., De Rafelis M., Brahmi C. and Chavagnac V. (2018) Sr isotope ratios of modern carbonate shells: Good and bad news for chemostratigraphy. *Geology* **46**, 1003–1006.

Elderfield H. (1986) Strontium isotope stratigraphy. *Palaeogeogr. Palaeoclimatol. Palaeoecol.* **57**, 71–90.

Edwards C. T., Saltzman M. R., Leslie S. A., Bergström S. M., Sedlacek A. R. C., Howard A., Bauer J. A., Sweet W. C. and Young S. A. (2015) Strontium isotope ($^{87}Sr/^{86}Sr$) stratigraphy of Ordovician bulk carbonate: implications for preservation of primary values. *GSA Bull.* **127**, 1275–1289.

Eldrett J. S., Minisini D. and Bergman S. C. (2014) Decoupling of the carbon cycle during Oceanic Anoxic Event 2. *Geology* **42**, 567–570.

Eldrett J. S., Ma C., Bergman S. C., Lutz B., Gregory F. J., Dodsworth P. and Kelly A. (2015a) An astronomically calibrated stratigraphic of the Cenomanian, Turonian and earliest Coniacian from the Cretaceous Western Interior Seaway, USA: Implications for global chronostratigraphy. *Cret. Res.* **56**, 316–344.

Eldrett J. S., Ma C., Bergman S. C., Ozkan A., Minisini D., Lutz B. and Kelly S. J. (2015b) Origin of limestone-marlstone cycles: Astronomic forcing of organic rich sedimentary rocks from the Cenomanian to early Coniacian of the Cretaceous Western Interior Seaway, USA. *Earth Planet. Sci. Lett.* **423**, 98–113.

Eldrett J. S., Dodsworth P., Bergman S. C., Wright M. and Minisini D. (2017) Water-mass evolution in the Cretaceous Western Interior Seaway of North America and Equatorial Atlantic. *Clim. Past* **13**, 855–878.

Frijia G. and Parente M. (2008) Strontium isotope stratigraphy in the upper Cenomanian shallow-water carbonates of the southern Apennines: short-term perturbations of marine $^{87}Sr/^{86}Sr$ during the oceanic anoxic event 2. *Palaeogeogr. Palaeoclimatol. Palaeoecol.* **261**, 15–29.

Hodell D. A., Mead G. A. and Mueller P. A. (1990) Variation in the strontium isotopic composition of seawater (8 Ma to present): implications for chemical weathering rates and dissolved fluxes to the oceans. *Chem. Geol.* **80**, 291–307.

Holmden C., Muehlenbachs K. and Creaser R. A. (1997a) Depositional environment of the early Cretaceous Ostracode Zone: Paleohydrologic constraints from O, C and Sr isotopes. In: Petroleum Geology of the Cretaceous Mannville Group, Western Canada. Eds. S. G. Pemberton and D. P. James. Canadian Society of Petroleum Geologists, Memoir 18.

Holmden C., Creaser R. A. and Muehlenbachs K. (1997) Paleosalinities in ancient brackish water systems determined by $^{87}Sr/^{86}Sr$ ratios in carbonate fossils: a case study from the Western Canada Sedimentary Basin. *Geochim. Cosmochim. Acta* **61**, 2105–2118.

Holmden C. and Hudson J. D. (2003) $^{87}Sr/^{86}Sr$ and Sr/Ca investigation of Jurassic molluscs from Scotland: Implications for paleosalinities and the Sr/Ca ratio of seawater. *GSA. Bull.* **115**, 1249–1264.

Holmden C., Papanastassiou D. A., Blanchon P. and Evans S. (2012) $\delta^{44/40}Ca$ variability in shallow water carbonates and the impact of submarine groundwater discharge on Ca-cycling in marine environments. *Geochim. Cosmochim. Acta* **83**, 179–194.

Huang K. F., You C. F., Chung C. H. and Lin I. T. (2011) Nonhomogeneous seawater Sr isotopic composition in the coastal oceans: a novel tool for tracing water masses and submarine groundwater discharge. *Geochem. Geophys. Geosyst.* **12**, 1–14.

Huber B. T., Norris R. D. and MacLeod K. G. (2002) Deep-sea paleotemperature record of extreme warmth during the Cretaceous. *Geology* **30**, 123–126.

Ingall E. D., Bustin R. M. and Van Cappellen P. (1993) Influence of water column anoxia on the burial and preservation of carbon and phosphorus in marine shales. *Geochim. Cosmochim. Acta* **57**(2), 303–316.

Ingall E. D. and Jahnke R. (1994) Evidence for enhanced phosphorus regeneration from marine-sediments overlain by oxugen depleted waters. *Geochim. Cosmochim. Acta* **58**, 2571–2575.

Ingram B. L., Coccioni R., Montanari A. and Richter F. M. (1994) Strontium isotopic composition of mid-Cretaceous seawater. *Science* **264**, 546–550.

Jacobson A. D., Blum J. D. and Walter L. M. (2002) Reconciling the elemental and Sr isotope composition of Himalayan weathering fluxes: Insights from the carbonate geochemistry of stream waters. *Geochim. Cosmochim. Acta* **66**, 3417–3429.

Jenkyns H. C. (2010) Geochemistry of oceanic anoxic events. *Geochem. Geophys. Geosyst.* **11**, Q03004.

Jenkyns H. C., Dickson A. J., Ruhl M. and van den Boorn S. H. J. M. (2017) Basalt–seawater interaction, the Plenus Cold Event, enhanced weathering and geochemical change: deconstructing Oceanic Anoxic Event 2 (Cenomanian–Turonian, Late Cretaceous). *Sedimentology* **64**, 16–43.

Jones C. E. and Jenkyns H. C. (2001) Seawater strontium isotopes, oceanic anoxic events, and seafloor hydrothermal activity in the Jurassic and Cretaceous. *Am. J. Sci.* **301**, 112–149.

Jones M. M., Sageman B. B., Selby D., Jicha B. R., Singer B. S. and Titus A. L. (2020) Regional chronostratigraphic synthesis of the Cenomanian-Turonian OAE 2 interval Western Interior Basin (USA): New Re-Os chemostratigraphy and 40Ar/39Ar geochronology. *GSA Bull.*

Kawahata H., Nohara M., Ishizuka H., Hasebe S. and Chiba H. (2001) Sr isotope geochemistry and hydrothermal alteration of the Oman ophiolite. *J. Geophys. Res. Solid Earth* **106**, 11083–11099.

Kristall B., Jacobson A. D. and Hurtgen A. T. (2017) Modeling the paleo-seawater radiogenic Sr isotope record: A case study of the Late Jurassic-Early Cretaceous. *Palaeogeogr. Palaeoclimatol. Palaeoecol.* **472**, 163–176.

Larson R. L. (1991) Latest pulse of the Earth: Evidence for a mid-Cretaceous superplume. *Geology* **19**, 547–550.

Leckie R. M., Bralower T. J. and Cashman R. (2002) Oceanic anoxic events and plankton evolution: Biotic response to tectonic forcing during the mid-Cretaceous. *Paleoceanography* **17**, 1041.

Li D., Shields-Zhou G. A., Ling H. F. and Thirlwall M. (2011) Dissolution methods for strontium isotope stratigraphy: Guidelines for the use of bulk carbonate and phosphorite rocks. *Chem. Geol.* **290**, 133–144.

McArthur J. M., Thirlwall M. F., Chen M., Gale A. S. and Kennedy W. J. (1993a) Strontium isotope stratigraphy in the late Cretaceous: Numerical calibration of the Sr isotope curve and intercontinental correlation for the Campanian. *Paleoceanography* **8**, 859–873.

McArthur J. M., Gale A. S., Kennedy W. J., Burnett J. A., Mattey D. and Lord A. R. (1993b) Strontium isotope stratigraphy for the Late Cretaceous: a new curve, based on the English chalk. In *High Resolution Stratigraphy* (eds. E. A. Hailwood and R. B. Kidd). Geological Society Special Publication No. 70, pp. 195–209.

McArthur J. M., Kennedy W. J., Chen M., Thirlwall M. F. and Gale A. S. (1994) Strontium isotope stratigraphy for Late Cretaceous time: Direct numerical calibration of the Sr isotope curve based on the US Western Interior. *Palaeogeogr. Palaeoclimatol. Palaeoecol.* **108**, 95–119.

McArthur J. M., Howarth R. J. and Schields G. A. (2012) Strontium isotope stratigraphy. In *The Geologic Time Scale* (eds. F. M. Gradstein, J. G. Ogg, M. D. Schmitz and G. M. Ogg). Elsevier, Amsterdam, pp. 207–232.

Minisini D., Eldrett J., Bergman S. C. and Forkner R. (2018) Chronostratigraphic framework and depositional environments in the organic-rich, mudstone-dominated Eagle Ford Group, Texas, USA. *Sedimentology* **65**, 1520–1557.

Monteiro F., Pancost R., Ridgwell A. and Donnadieu Y. (2012) Nutrients as the dom-inant control on the spread of anoxia and euxinia across the Cenomanian-Turonian oceanic anoxic event (OAE 2): model–data comparison. *Paleoceanography* **27**, PA4209.

Montanez I. P., Banner J. L., Osleger D. A., Borg L. E. and Bosserman P. J. (1996) Integrated Sr isotope variations and sea-level history of Middle to Upper Cambrian platform carbonates: implications for the evolution of Cambrian seawater $^{87}Sr/^{86}Sr$. *Geology* **24**, 917–920.

Orth C. J., Attrep, Jr., M., Quintana L. R., Elder W. P., Kauffman E. G., Diner R. and Villamil T. (1993) Elemental abundance anomalies in the late Cenomanian extinction interval: a search for the source(s). *Earth Planet. Sci. Lett.* **117**, 189–204.

Ostrander C. M., Owens J. D. and Nielsen S. G. (2017) Constraining the rate of oceanic deoxygenation leading up to a Cretaceous Oceanic Anoxic Event (OAE-2: 94 Ma). *Sci. Adv.* **3**, 1–5.

Owens J. D., Lyons T. W. and Lowery C. M. (2018) Quantifying the missing sink for global organic carbon burial during a Cretaceous oceanic anoxic event. *Earth Planet. Sci. Lett.* **499**, 83–94.

Oxburgh R. (2001) Residence time of osmium in the oceans. *Geochem., Geophys. Geosyst.* **2**.

Palmer M. R. and Edmond J. M. (1989) The strontium isotope budget of the modern ocean. *Earth Planet. Sci. Lett.* **92**, 11–26.

Pedersen T. F. and Calvert S. E. (1990) Anoxia vs. productivity: What controls the formation of organic-carbon-rich sediments and sedimentary rocks?. *AAPG Bull.* **74**, 454–472.

Peucker-Ehrenbrink B. and Fiske G. J. (2019) A continental perspective of the seawater $^{87}Sr/^{86}Sr$ record: a review. *Chem. Geol.* **510**, 140–165.

Pogge von Strandmann P. A. E., Jenkyns H. C. and Woodfine R. G. (2013) Lithium isotope evidence for enhanced weathering during Oceanic Anoxic Event 2. *Nat. Geosci.* **6**, 668–672.

Pratt L., Force E. R. and Pomerol B. (1991) Coupled manganese and carbono-isotopic events in marine carbonates at the Cenomnanian-Turonian boundary. *J. Sed. Pet.* **61**, 370–383.

Renard M. (1986) Pelagic carbonate chemostratigraphy (Sr, Mg, $^{18}0$, ^{13}C). *Mar. Micropaleontol.* **10**, 117–164.

Richter F. M., Rowley D. B. and DePaolo D. (1992) Sr isotope evolution of seawater: the role of tectonics. *Earth Planet. Sci. Lett.* **109**, 11–23.

Richter F. M. and Liang Y. (1993) The rate and consequences of Sr diagenesis in deep-sea carbonates. *Earth Planet. Sci. Lett.* **117**, 553–565.

Sageman B. B., Meyers S. R. and Arthur M. A. (2006) Orbital time scale and new C-isotope record for Cenomanian-Turonian boundary stratotype. *Geology* **34**, 125–128.

Schlanger S. O. and Jenkyns H. C. (1976) Cretaceous oceanic anoxic events: Causes and consequences. *Geol. Mijnbouw* **55**, 179–184.

Scholle P. A. and Arthur M. A. (1980) Carbon isotope fluctuations in Cretaceous pelagic limestones: Potential stratigraphic and petroleum exploration tool. *AAPG Bull.* **64**, 67–87.

Sinton C. W. and Duncan R. A. (1997) Potential links between ocean plateau volcanism and global ocean anoxia at the Cenomanian-Turonian boundary. *Econ. Geol.* **92**, 836–842.

Snow L. J., Duncan R. A. and Bralower T. J. (2005) Trace element abundances in the Rock Canyon Anticline, Pueblo, Colorado, marine sedimentary section and their relationship to Caribbean plateau construction and oxygen anoxic event 2. *Paleoceanography* **20**, PA3005.

Steuber T. and Veizer J. (2002) Phanerozoic record of plate tectonic control of seawater chemistry and carbonate sedimentation. *Geology* **30**, 1123–1126.

Sugarman P. J., Miller K. G., Burky D. and Feigenson M. D. (1995) Uppermost Campanian-Maestrichtian strontium isotopic, biostratigraphic, and sequence stratigraphic framework of the New Jersey Coastal Plain. *GSA Bull.* **107**, 19–37.

Sullivan D. L., Brandon A. D., Eldrett J., Bergman S. C., Wright S. and Minisini D. (2020) High resolution osmium data record three distinct pulses of magmatic activity during cretaceous Oceanic Anoxic Event 2 (OAE-2). *Geochim. Cosmochim. Acta* **285**, 257–273.

Sun H., Xiao Y. L., Gao Y., Zhang G., Casey J. F. and Shen Y. (2018) Rapid enhancement of chemical weathering recorded by extremely light seawater lithium isotopes at the Permian-Triassic boundary. *Proc. Natl. Acad. Sci.* **115**, 3782–3787.

Them T. R., Gill B. C., Caruthers A. H., Gerhardt A. M., Gröcke D. R., Lyons T. W., Mar-roqui´n S. M., Nielsen S. G., Trabucho Alexandre J. P. and Owens J. D. (2018) Thallium isotopes reveal protracted anoxia during the Toarcian (Early Jurassic) associated with volcanism, carbon burial, and mass extinction. *Proc. Natl. Acad. Sci.* https://doi.org/10.1073/pnas.1803478115.

Topper R. P. M., Trabucho Alexandre J., Tuenter E. and Meijer P. T. (2011) A regional ocean circulation model for the mid-Cretaceous North Atlantic Basin: implications for black shale formation. *Clim. Past* **7**, 277–297.

Trabucho-Alexandre J., Tuenter E., Henstra G. A., van der Zwan K. J., van de Wal R. S. W., Dijkstra H. A. and de Boer P. L. (2010) The mid-Cretaceous North Atlantic nutrient trap: Black shales and OAEs. *Paleoceanography* **25**, PA4201.

Tribovillard N., Algeo T. J., Lyons T. and Riboulleau A. (2006) Trace metals as paleoredox and paleoproductivity proxies: an update. *Chem. Geol.* **232**, 12–32.

Turgeon S. C. and Creaser R. A. (2008) Cretaceous Anoxic Event 2 triggered by a massive magmatic episode. *Nature* **454**, 323–326.

Vérard C., Hochard C., Baumgartner P. O. and Stampfli G. M. (2015) 3Dpalaeogeographic reconstructions of the Phanerozoic versus sea-level and Sr-ratio variations. *J. Palaeogeogr.* **4**, 64–84.

Veizer, J. (1983) Trace elements and isotopes in sedimentary carbonates, In Carbonates: Mineralogy and Chemistry. Reviews in Mineralogy (ed. R. J. Reeder) 11, 265–300.

Wallmann K. (2001) Controls on the Cretaceous and Cenozoic evolution of seawater composition, atmospheric CO2 and climate. *Geochim. Cosmochim. Acta* **65**, 3005–3025.

Wickman F. E. (1948) Isotope ratios: a clue to the age of certain marine sediments. *J. Geol.* **56**, 61–66.

Young S. A., Saltzman M. R., Foland K. A., Linder J. S. and Kump L. R. (2009) A major drop in seawater 87Sr/86Sr during the Middle Ordovician (Darriwilian): Links to volcanism and climate?. *Geology* **37**, 951–954.

Zhang S. and DePaolo D. J. (2020) Equilibrium calcite-fluid Sr/Ca partition coefficient from marine sediment and pore fluids. *Geochim. Cosmochim. Acta* **289**, 33–46.

Associate editor: Andrew D. Jacobson